Zeitschrift: Schweizerische mineralogische und petrographische Mitteilungen = Bulletin suisse de minéralogie et pétrographie

Band: 79 (1999)

Heft: 2

Artikel: Metamorphic and tectonic evolution of Austroalpine units at the western margin of the Gurktal nappe complex, Eastern Alps

Autor: Koroknai, Balázs / Neubauer, Franz / Genser, Johann

DOI: https://doi.org/10.5169/seals-60209

SCHWEIZ. MINERAL. PETROGR. MITT. 79, 277–295, 1999

Metamorphic and tectonic evolution of Austroalpine units at the western margin of the Gurktal nappe complex, Eastern Alps

by *Balázs Koroknai*[1,2], *Franz Neubauer*[1], *Johann Genser*[1] and *Dan Topa*[1]

Abstract

Petrological and structural investigations were carried out on samples of Middle and Upper Austroalpine units at the western edge of the Gurktal nappe complex, Eastern Alps (Nock mountains). Based on thermobarometric calculations applied to garnet-plagioclase-muscovite-biotite parageneses, the Alpine metamorphic conditions in the Middle Austroalpine crystalline basement (Radenthein and Bundschuh nappes) can be estimated at ca. 600 °C and 10–11 kbar within the upper epidote-amphibolite facies. Moreover, the presence of an earlier stage with even higher pressure is likely. Pre-Alpine (probably Variscan) relic mineral parageneses are not preserved in some of the investigated Middle Austroalpine rocks. Calcite-dolomite thermometry in the Upper Austroalpine (Murau nappe) yielded temperatures of ca. 460–500 °C, which is interpreted to represent Alpine metamorphic conditions in contrast to temperatures of 550–600 °C from garnet-biotite thermometry which are assumed to indicate pre-Alpine metamorphic conditions. Garnet-biotite parageneses were later strongly overprinted by retrogression within greenschist facies conditions. The break in metamorphic P-T conditions between Middle Austroalpine units and the Murau nappe is considered to result from Late Cretaceous low-angle normal faulting that juxtaposed these two units along a ductile shear zone with top-to-ESE displacement.

Keywords: detachment faulting, geothermobarometry, shear zone, Cretaceous, Austroalpine, Gurktal nappe complex.

1. Introduction

Crustal-scale nappe assembly within collisional orogens regularly leads to burial and metamorphic overprint of crustal fragments (e.g., ENGLAND and THOMPSON, 1984). Subsequent extensional processes result in exhumation of previously buried crustal units. Vertical motion in relation to the Earth's surface can be, therefore, monitored by changing metamorphic pressure conditions. Furthermore, varying metamorphic pressure-temperature conditions can be used to distinguish individual tectonic bodies, e.g. nappes and extensional allochthons.

This paper is dealing with the structural and metamorphic relationships between the Middle and Upper Austroalpine nappe units along the western margin of the Gurktal nappe complex (Upper Austroalpine units) in the Eastern Alps (Fig. 1) that show strongly contrasting metamorphic pressure-temperature conditions of the penetrative Cretaceous overprint (e.g., FRANK, 1987; SCHIMANA, 1986). New structural, textural and petrological data are used to constrain the Cretaceous tectonic processes of that region where previous data suggest Late Cretaceous extension (e.g., RATSCHBACHER et al., 1990).

2. Geological setting

The Austroalpine units within the Eastern Alps form a coherent sheet composed of a number of nappes that were assembled during Late Cretaceous nappe stacking under ductile strain and a wide spectrum of metamorphic pressure-temperature conditions (e.g., FRANK, 1987; TOLLMANN, 1987, RATSCHBACHER and NEUBAUER, 1989).

[1] Institut für Geologie und Paläontologie der Paris-Lodron-Universität Salzburg, Hellbrunner Str. 34, A-5020 Salzburg, Austria. Corresponding author: Franz Neubauer <franz.neubauer@sbg.ac.at>

[2] Present address: Academic Research Group, Eötvös Lórand University, Múzeum krt. 4/A, H-1088 Budapest, Hungary.

Available data show that penetrative internal deformation occurred during the Cretaceous (e.g., FRANK et al., 1987; DALLMEYER et al., 1996), partly associated with high pressure metamorphism up to eclogite facies (ca. 18 kbar; MILLER, 1990; EHLERS et al., 1994; FROITZHEIM et al., 1996, for review). Major portions of these units are interpreted to represent lower plate sequences emplaced during Cretaceous subduction of Austroalpine continental crust beneath Meliata-like oceanic tectonic elements (NEUBAUER, 1994; DALLMEYER et al., 1996, 1998). Late Cretaceous exhumation led to crustal thinning and cooling of previously overthickened crust (RATSCHBACHER et al., 1989; NEUBAUER et al., 1995; DALLMEYER et al., 1998). Subsequent Tertiary piggy-back emplacement of these units onto Penninic units did not lead to major internal deformation of Austroalpine units.

Eastward of the Penninic Tauern window, all major Austroalpine units are exposed in the classical Bundschuh area where HOLDHAUS (1921), based on fossil discoveries, argued for an intra-Austroalpine nappe structure (Fig. 1b). Here, the Austroalpine units comprise from bottom to top (TOLLMANN, 1975, 1977; SCHIMANA, 1986; NEU-

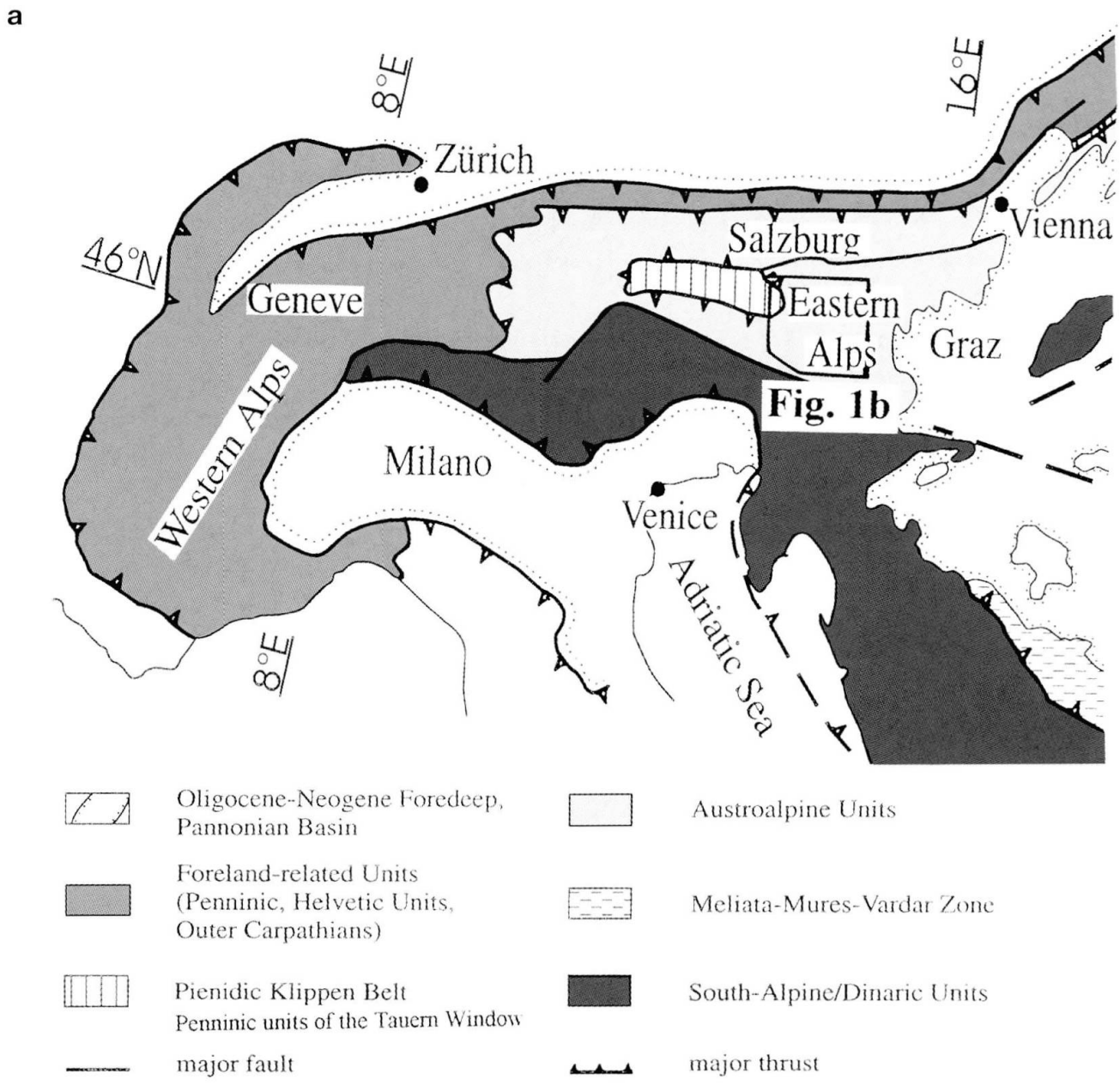

Fig. 1 (a) Schematic tectonic overview of the Eastern Alps with location of the investigated area. (b) Simplified geological map showing general geological relationships of the Gurktal nappe complex / Gurktal extensional allochthon to underlying units.

BAUER, 1987; NEUBAUER and PISTOTNIK, 1984; VON GOSEN, 1989): (1) the Radenthein micaschist complex (RMC), a basement complex constituting the Radenthein nappe; (2) the Bundschuh nappe including the Bundschuh complex (BC), a gneissic, pre-Permian basement unit, and a Permian to Mesozoic cover sequence (Stangalm Group); Radenthein and Bundschuh nappes are classically interpreted to represent Middle Austroalpine units; (3) the Murau nappe with a phyllitic Palaeozoic basement; and (4) the Stolzalpe nappe also with a phyllitic Palaeozoic basement, and Late Carboniferous to Triassic cover sequences. Murau and Stolzalpe nappes are part of the Gurktal nappe complex (Upper Austroalpine nappe complex).

The present superposition of the Gurktal nappe complex over Middle Austroalpine units is interpreted to result from Cretaceous nappe stacking within ductile deformational conditions (TOLLMANN, 1977; NEUBAUER, 1980, 1987; RATSCHBACHER and NEUBAUER, 1989; VON GOSEN, 1989) although there is a wide disagreement on the nature and extent of displacement (e.g., CLAR, 1965; TOLLMANN, 1975; FRANK, 1987; FRIMMEL, 1986 a, b; 1988). Based on scarce shear

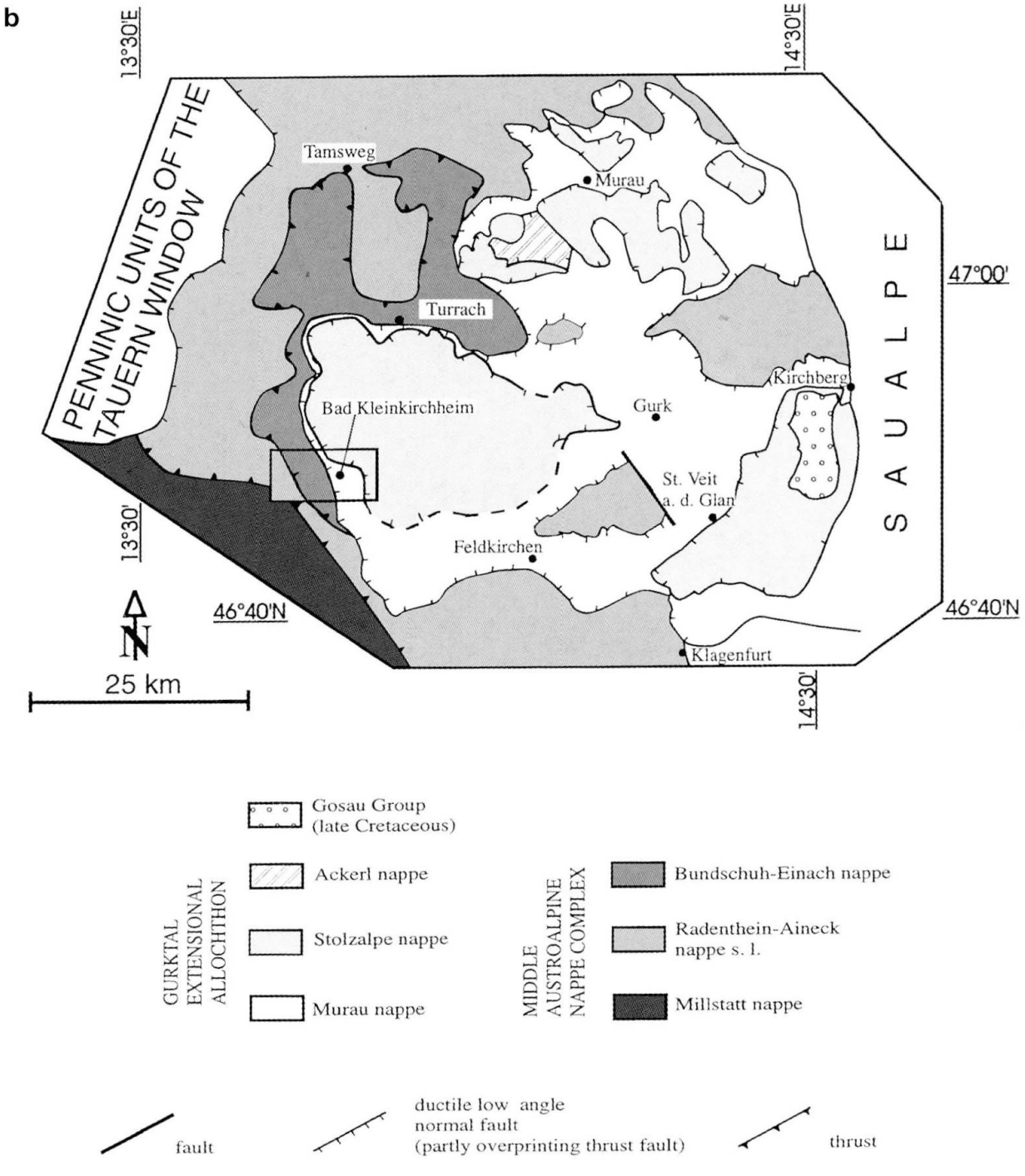

sense criteria a top to the W (WNW) displacement of hangingwall units was proposed (NEUBAUER, 1987; RATSCHBACHER and NEUBAUER, 1989; RATSCHBACHER et al., 1989; VON GOSEN, 1989). Furthermore, many structural data favour an overprint by a second ductile phase with a general top to the ESE displacement (NEUBAUER, 1987) that was interpreted to represent subsequent Late Cretaceous east-directed motion due to extension (RATSCHBACHER et al., 1989, 1990; STOCK, 1992; ANTONITSCH and NEUBAUER, 1992). The second event was also interpreted to be responsible for a break in the Cretaceous peak metamorphic conditions between the Middle Austroalpine units / Murau nappe and the overlying Stolzalpe nappe (NEUBAUER, 1980; RATSCHBACHER et al., 1990).

These units were studied and sampled along an approximately 10 km long, E–W oriented section between Radenthein and Patergassen, which include all units from the Radenthein nappe to the Stolzalpe nappe (Fig. 2). The schematic tectonic stratigraphy of these units is shown in figure 3.

3. Analytical methods

Fault and striae field data have been processed for palaeostress orientation analysis following the inversion methods described by ANGELIER and MECHLER (1977; see compilation in MESCHEDE, 1995). The program "Gefüge 5" (WALLBRECHER and UNZOG, 1993) was used for graphical representation of the tectonic data. Evaluation of shear senses follows methods described by, e.g., SIMPSON and SCHMID (1983), CHOUKROUNE et al. (1987), PETIT (1987) and HANMER and PASSCHIER (1991). Microfabrics and textures were studied on orient-

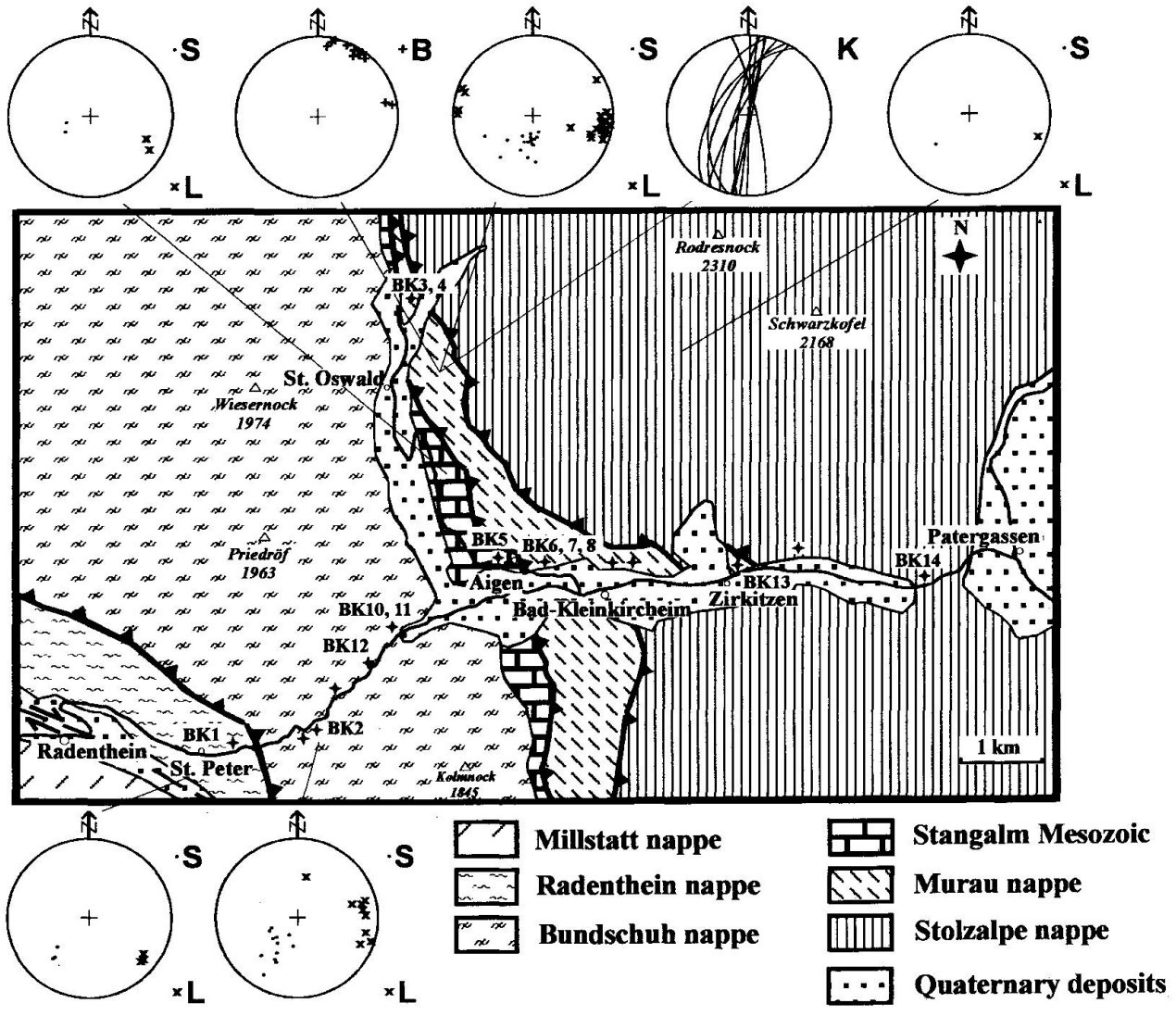

Fig. 2 Simplified structural map of the investigated area showing outcrop localities and main structural elements. Location is shown on figure 1b. S – foliation, L – stretching lineation, B – fold axis, K – tension gash. Lambert projection, lower hemisphere.

ed samples with standard universal stage techniques.

Mineral chemistry of selected samples were determined with a JEOL JXA-8600 microprobe. Standard conditions were: 15 kV acceleration voltage; 20 nA sample current. Raw data were corrected using standard ZAF correction procedures.

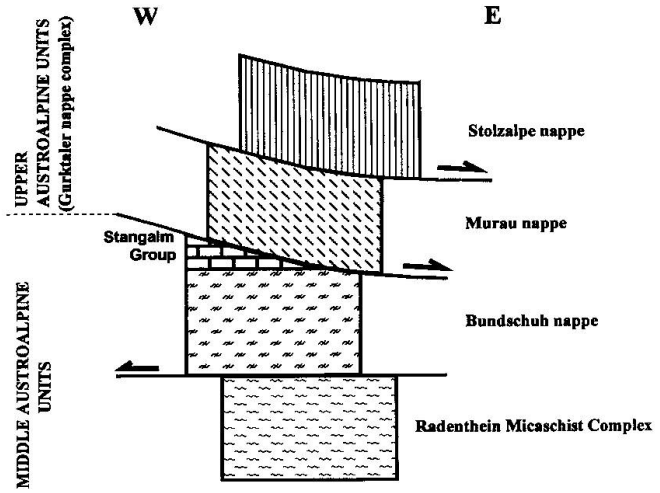

Fig. 3 Schematic tectonic stratigraphy of the investigated area.

4. Results

4.1. STRUCTURAL INVESTIGATIONS

Two sets of structures have been observed in all tectonic units (along the Radenthein–Patergassen section; Fig. 2): (1) penetrative ductile structures that formed within peak and/or retrogressive metamorphism; and (2) late-stage brittle structures that overprinted the earlier ones.

The lithologic members of the upper portions of the Radenthein micaschist complex show a flat-lying, NE-dipping, penetrative foliation and associated ESE-plunging stretching lineation (Fig. 2). These rocks are generally well-recrystallized and do not show retrogression.

Paragneisses and micaschists of the Bundschuh nappe as well as marbles of the Stangalm Group also include a gently NE-dipping penetrative foliation, and an associated E- to ESE-plunging stretching lineation. The foliation of the Murau and Stolzalpe nappes gently dips to the N to NE, while the associated stretching lineation trends mostly E (Fig. 2). The foliation of phyllitic rocks within the Murau nappe is penetrative to closely spaced, and comprises fine ribbon quartz and sericitic layers. Shear bands are common within phyllitic units and indicate E- to ESE-directed shear. The penetrative foliation is refolded into open, upright NNE-plunging folds that also contain a widely spaced axial surface foliation. Subvertical N-trending tension gashes are common within the Murau nappe. They indicate approximately E–W oriented, (sub)horizontal extension. Both, open upright folds and steep tension gashes also occur within the Bundschuh nappe.

Mesoscale faults and striae are common both in the upper portions of the Bundschuh nappe and in the Murau nappe (Fig. 4). In general, they are dominated by a conjugate set of ENE respectively NW-dipping normal faults. Resulting palaeostress orientation patterns indicate a subvertical orientation of σ_1 and a subhorizontal WNW-trending σ_3 direction due to WNW–ESE stretching of rocks (Fig. 4).

4.2. MICROFABRICS AND TEXTURES

Rotated σ-porphyroclasts of garnet and intrafolial folds in the Radenthein nappe show top-to-the W transport (Fig. 5a). The orientation of tensional fractures between garnet fragments indicates ca. ESE–WNW orientated stretching. Crenulation of the foliation can be observed, too. Quartz c-axes patterns of some lithologic units from the Radenthein nappe are unusual and display a small circle distribution around the Y direction (Fig. 6).

The rocks of the Bundschuh Complex rocks are well-recrystallized and annealed, and do not contain a preferred orientation of quartz c-axes (Fig. 6). Well-developed shear indicators are missing in this unit.

In the Murau nappe, sample BK3, which is a very well-developed quartz mylonite, shows a prominent preferred quartz c-axes orientation. Shear bands and S-C fabrics, indicating top to the ESE shear, are common within this type of mylonite (Fig. 7 a, b). For other studied rocks (samples BK6, 8, and 14 from the Murau and Stolzalpe nappes), no preferred quartz c-axes orientation could be observed (Fig. 6). Shear bands and asymmetrical pressure shadows around garnets are also characteristic for the Murau nappe (Fig. 5c). Occasionally, normal slip crenulation and asymmetrical foliation boudinage occur as well. These indicators show mostly top-to-the E to ESE transport. Boudinaged white mica indicates E–W stretching, too.

Grain boundaries in quartz layers and lenses of rocks exposed within the Murau nappe are dentate to lobate in most cases, recording synmetamorphic deformation. Elongated grains, undulose extinction, deformation lamellae and mortar tex-

ture also record strong deformation after peak-temperature metamorphism (Fig. 5d). However, well-equilibrated grain boundaries are also present in some samples. These are interpreted to represent remnants of an earlier stage and suggest strain partitioning within the Murau nappe during the last deformation stage. Feldspar and garnets often appear as rigid porphyroclasts (0.2–0.7 mm) with pressure shadows in rocks of the Murau nappe, but also small (0.01–0.1 mm) well-recrystallized grains, often with optically strain-free properties, can be observed.

These relationships suggest that the rocks of Bundschuh nappe are mostly annealed. In contrast, quartz of rocks from the Murau nappe is heavily deformed under low-temperature plasticity conditions.

4.3. PETROLOGICAL INVESTIGATIONS

Representative mineral analyses of various samples are given in tables 1–3.

Garnet is a characteristic metamorphic mineral in these rocks and therefore numerous profiles were measured from several locations and tectonic units. Metamorphic conditions were determined on the basis of equilibrium mineral para-

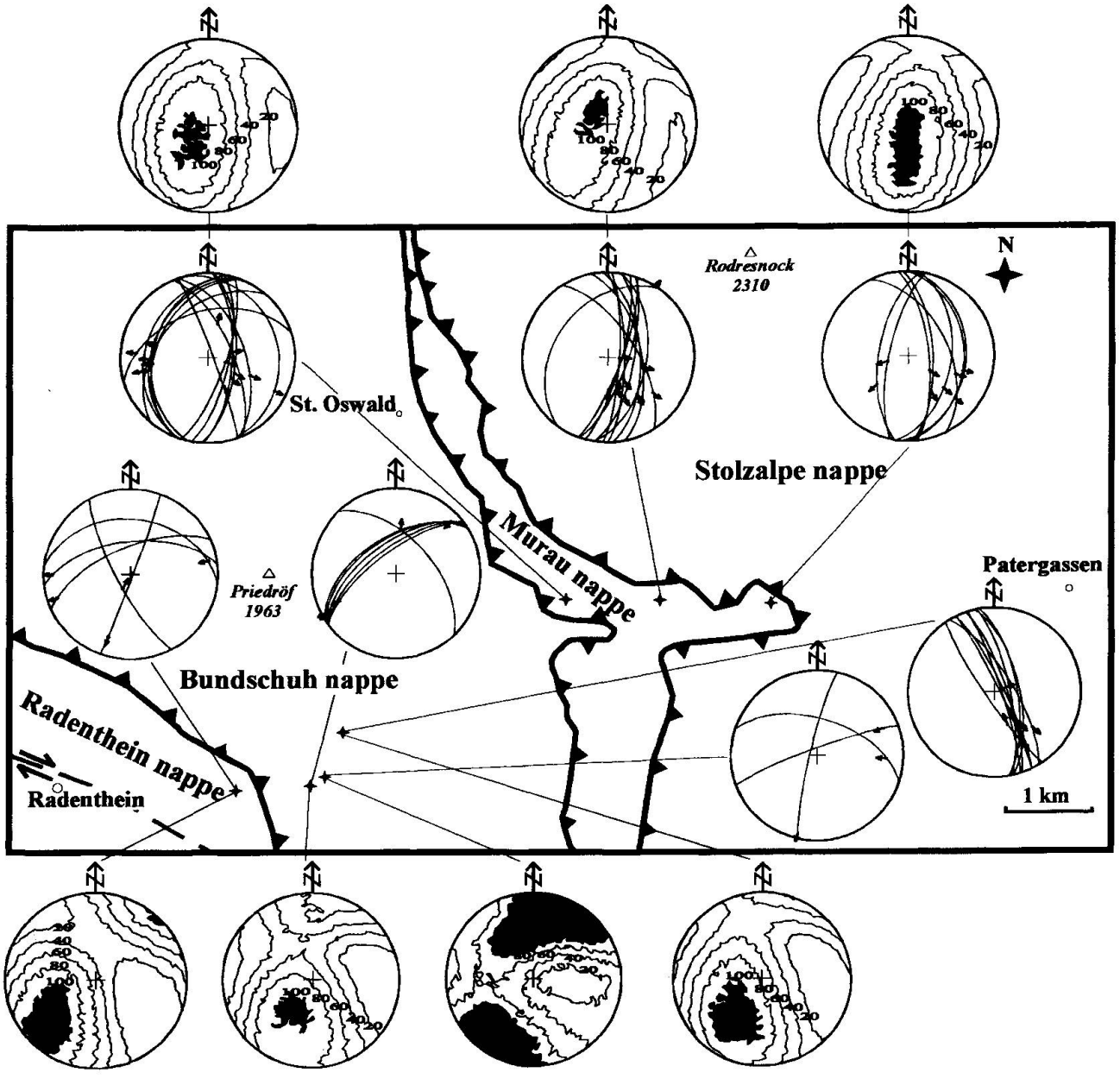

Fig. 4 Orientations of faults and striae and deduced palaeostress orientations (diagrams outside map). Lambert projection, lower hemisphere. Legend of palaeostress projections: Black – possible maximum principal stress orientation; stippled – possible minimum principal stress orientation.

geneses in each tectonostratigraphic unit, concentrating on the Middle Austroalpine crystalline basement (Radenthein and Bundschuh nappes). We applied Tweeq (BERMAN, 1991) and Thermocalc programs (POWELL and HOLLAND, 1988) for the calculation of P-T conditions, using, among others, also the calibrations of KLEEMANN and REINHARDT (1994), HOISCH (1991) and HODGES and CROWLEY (1985), respectively, on mineral assemblages which are in textural equilibrium. The results are compiled in table 5 for overview. The activity models used for Tweeq were from BERMAN (1990) for garnet, from FUHRMANN and LINDSLEY (1988) for feldspar, from CHATTERJEE and FROESE (1975) for mica, and from MCMULLIN et al. (1991) for biotite. In Thermocalc we used the activity models inherent from the supplementary program AX. The chosen activity model of paragonite which is present as a component in white mica in a considerable, but variable amount largely influences the results. Omitting paragonite, however, from Thermocalc calculations results in a large deviations on P-T conditions. Some representative thermodynamic input data are given in table 4. (The complete sets of input data can be received on request from the first author.) As examples, results of P-T estimates using the calibrations of KLEEMANN and REINHARDT (1994), HOISCH (1991) and HODGES and CROWLEY (1985) for chemical compositions presented in table 4 are shown in table 5, too.

4.3.1. Radenthein nappe

The essential rock type of the Radenthein nappe is a well-foliated, medium-grained, porphyrolepidoblastic garnet-micaschist. Garnet forms cracked, fragmented porphyroclasts of sizes of 0.5–3 mm wrapped around by the foliation. The internal foliation S_i is marked by small (0.01–0.1 mm) quartz inclusions within the garnets. The foliation is constituted by alternating biotite and muscovite (0.4–4 mm) and thin "ribbon quartz"

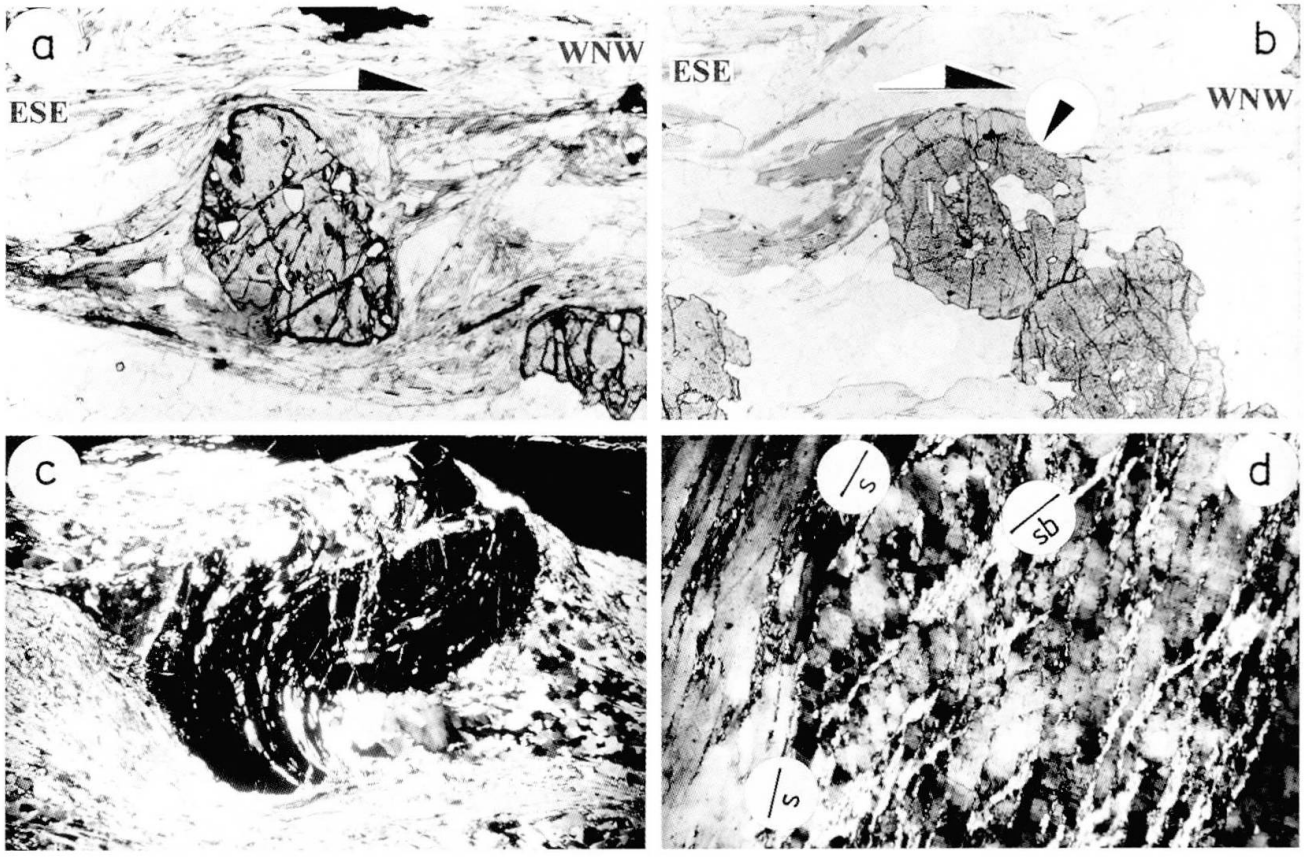

Fig. 5 Comparison of microfabrics in the Middle and Upper Austroalpine units: (a) Mantled garnet from the Radenthein micaschist with asymmetric quartz tails indicating top-to-the-WNW shear (BK1). (b) Zoned garnet from a gneiss of the Bundschuh nappe (BK10). (c) Garnet-bearing quartz-phyllite with σ-type garnet porphyroclast indicating top-to-the-E transport. Note the wrapping of foliation around the garnet (Gurktaler phyllite of the Murau nappe, sample BK7). (d) quartz microfabric of the Murau nappe (sample BK3). Note large elongated quartz grains and formation of shear bands with recrystallized small quartz grains. Long edge of all four photomicrographs: ca. 4 mm. Crossed polarizers.

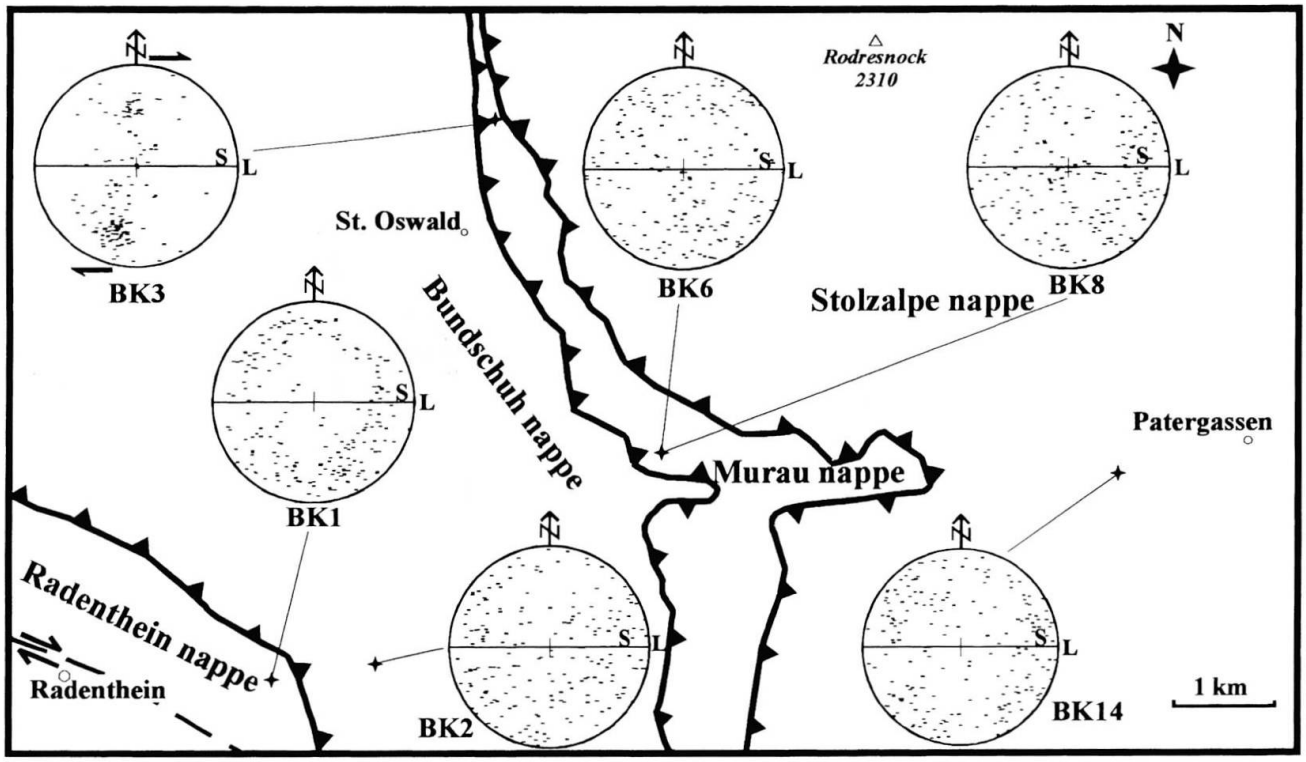

Fig. 6 Quartz c-axes diagrams.

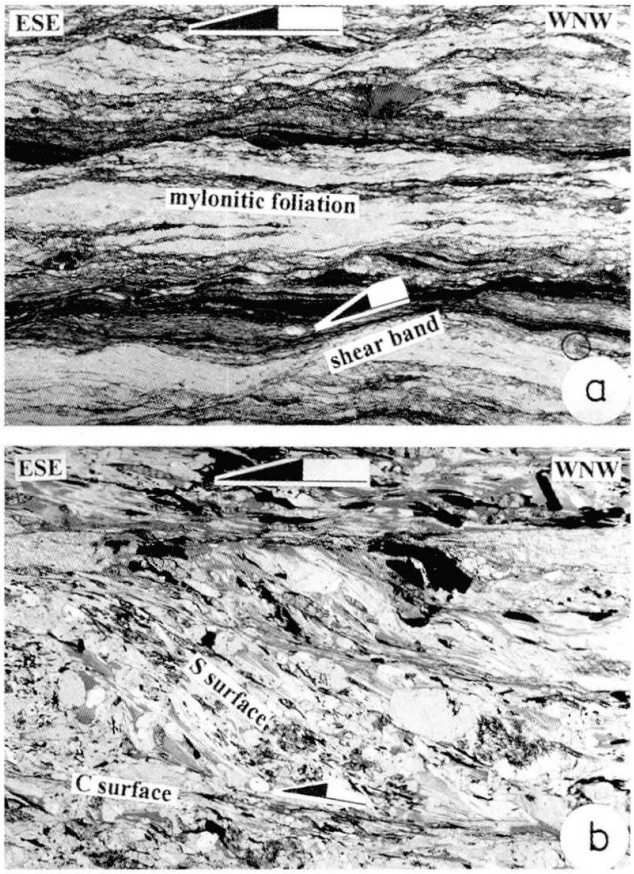

Fig. 7 Examples of microstructures indicating top-to-the-ESE displacement within the Murau nappe. (a) Mylonitic quartzphyllite with shear bands. (b) S-C fabrics. Long edge of both photomicrographs: ca. 4 mm. Crossed polarizers.

layers. Micas overgrowing the foliation are also present in small quantities. Chlorite only occurs sporadically, filling fissures between garnet fragments or forming thin rims around them. Feldspar is very rare as well. Zircon, rutile and a not identified yttrium-oxide are frequent as inclusions in micas. Further accessories are tourmaline, apatite, titanite, pyrite and ilmenite.

According to microprobe measurements, sample BK1 muscovite contains many very thin Na-rich lamellae (paragonite). They seem to be in equilibrium with muscovite (normal, straight grain boundaries) and are not an alteration product.

Garnets show no optical zonation. Their chemical composition is dominated by almandine (X_{Alm}: 0.803, X_{Py}: 0.132, X_{Gr}: 0.56, X_{Sp}: 0.09, rim-analysis). The element distribution (Fig. 8 a, b) shows normal zonation: FeO and MgO contents increase (FeO: 33.8–36.4 wt%; MgO: 2.13–4.01 wt%), while CaO and MnO contents decrease (CaO: 3.8–1.69 wt%; MnO: 3.5–0.49 wt%) from the center to the edge of the grain (in the case of CaO this trend is less well-expressed than that for MnO).

Garnet-biotite thermometry gives a temperature of ca. 600 °C for a pressure of 11 kbar (Tweeq). Calculations with Thermocalc using the garnet-biotite-muscovite mineral assemblage yields T = 627 ± 117 °C, P = 11.0 ± 2.6 kbar.

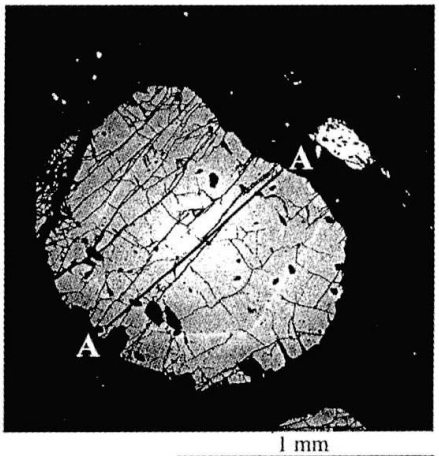

a

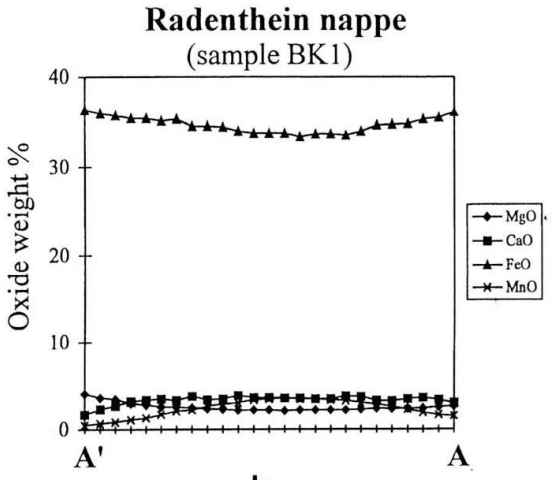

b

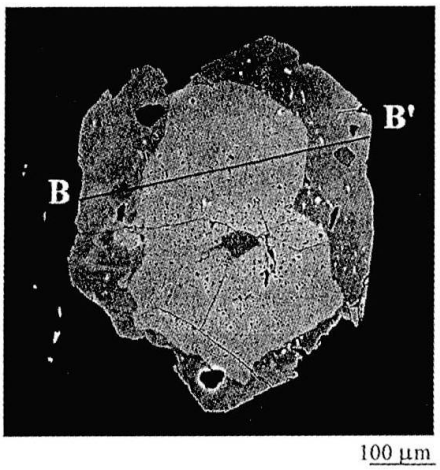

c

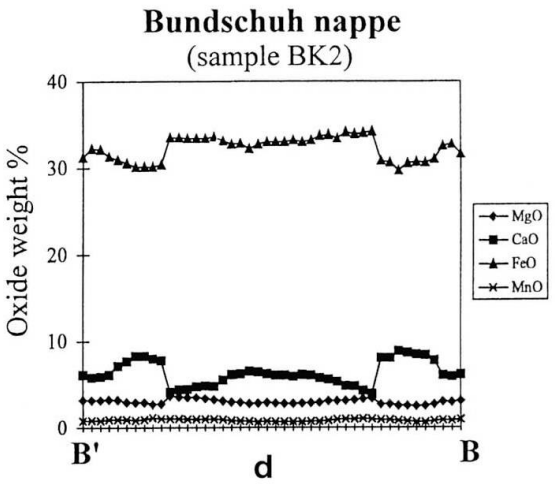

d

e

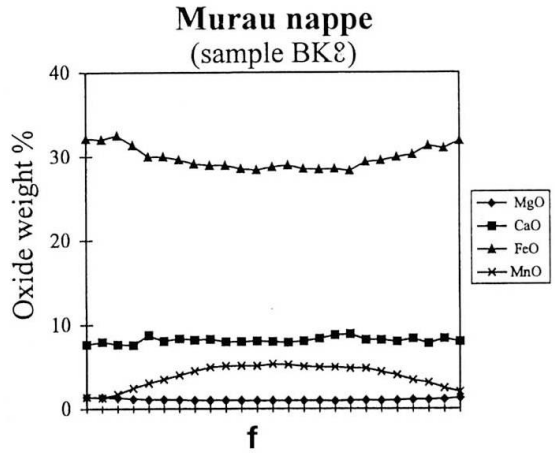

f

Fig. 8 Representative chemical composition of garnet from the Radenthein, Bundschuh and Murau nappes. (a) Back-scattered electron image of garnet in BK1 (Radenthein nappe). No core-rim structure is developed. (b) Element distribution in BK1. Length of section line is shown in figure 8a. (c) Back-scattered electron image of garnet in BK2 (Bundschuh nappe). Note the characteristic core-rim structure. (d) Element distribution in BK2. Section line is shown in figure 8c. (e) Relative intensity distribution for Ca–K_α X-ray line in the same grain. Note the three garnet generations. (f) Element distribution in BK8. Length of section line is ca. 4.5 mm, analyzed grain is not shown. Murau nappe.

Tab. 1 Representative mineral analyses from sample BK1, Radenthein nappe.

	Garnet		*Biotite*	*Muscovite*	*Paragonite*	*Chlorite*
	edge	*center*				
SiO_2	37.00	36.60	35.70	46.70	45.70	24.60
Al_2O_3	21.00	20.70	19.20	32.70	38.60	21.90
MgO	4.01	2.21	10.60	1.49	0.09	14.70
FeO	36.40	33.80	19.30	1.36	0.27	24.20
CaO	1.69	3.57	< 0.01	< 0.02	0.20	0.06
MnO	0.49	3.40	< 0.03	< 0.01	< 0.02	0.09
Na_2O	–	–	0.32	1.35	6.70	0.00
K_2O	–	–	8.20	9.20	1.26	< 0.01
TiO_2	< 0.01	< 0.03	0.98	0.51	0.15	< 0.04
Cr_2O_3	–	–	0.03	< 0.03	< 0.02	< 0.01
BaO	–	–	0.06	0.16	< 0.01	< 0.06
Cl	–	–	0.0	< 0.01	< 0.01	0.00
Total	100.54	100.21	94.38	93.46	92.94	85.52

4.3.2. Bundschuh nappe

Four paragneiss (BK2, BK10) and micaschist (BK11, BK12) samples of the Bundschuh nappe have been investigated in detail. Mineral assemblages – characterized by garnet, plagioclase, biotite, muscovite, paragonite, chlorite, quartz, ± phengite – are very similar in all these rocks. Paragneiss samples contain more feldspar (ca. 20–30 modal percent) than micaschists, some variations in chlorite content are also present.

Paragneisses are not well foliated, garnet forms cracked, hypidiomorphic to idiomorphic grains of 0.2–3 mm in BK2, while garnets in BK10 are idiomorphic, but their size is only ca. 0.1–0.4 mm. An optically zoned internal structure can be observed often, with a thin, frequently optically anomalous rim (see Fig. 5b) around the core. Garnets from BK2 contain small (0.01–0.1 mm) quartz inclusions. Accessories (partly also as inclusions in garnet and mica) are rutile, zircon, apatite, titanite, ilmenite, and pyrite.

In the well-foliated micaschists, garnets have diameters of 0.2–4 mm. They are often wrapped around by the foliation. In sample BK11, garnets are mostly small (0.1–0.4 mm) and idiomorphic (like in BK10) but some larger (up to 3.5 mm), strongly fragmented grains are also present. Accessories are the same as those within the paragneisses.

Feldspars form idiomorphic, tabular, frequently twinned crystals of 0.1–2 mm in BK2 while in BK10 they always occur in fine-grained (0.05–0.4 mm) aggregates consisting of quartz and micas. In the micaschists, they form generally idiomorphic grains of 0.1–0.8 mm. Some alteration of feldspar to sericite can be observed occasionally.

In the micaschists, the foliation is constituted by the alternation of strongly elongate and de-

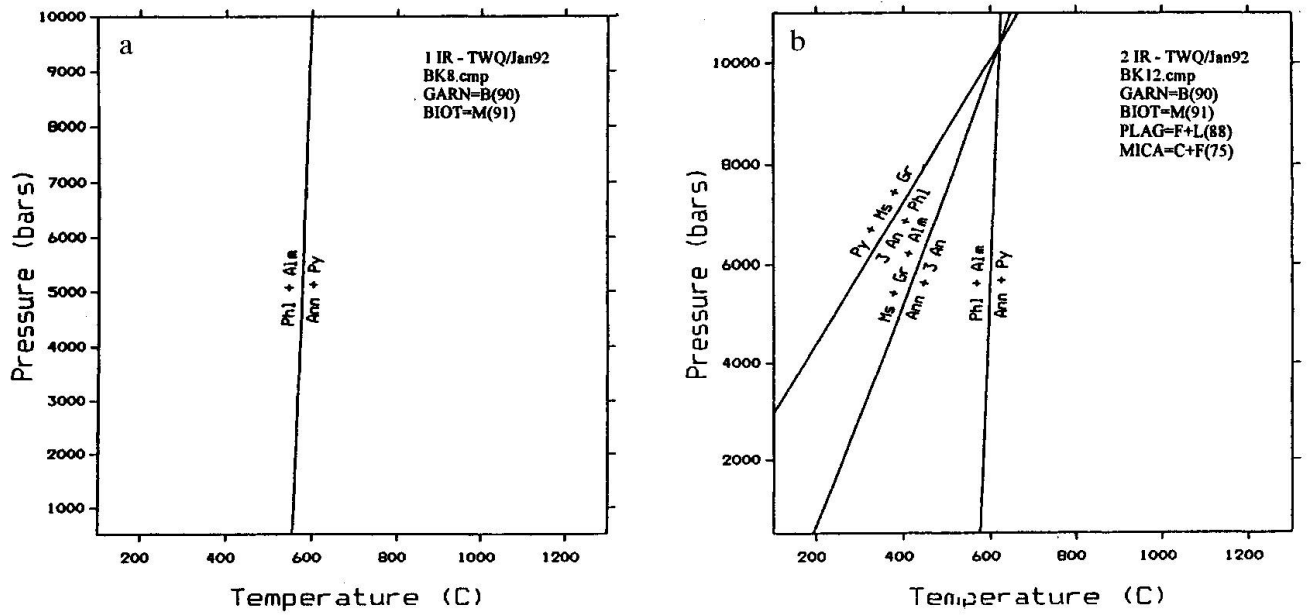

Fig. 9 Representative examples of thermobarometric results obtained from the Tweeq program. (a) BK8: Garnet-biotite thermometry, and (b) BK12: garnet-biotite-muscovite-plagioclase thermobarometry.

Tab. 2 Representative mineral analyses from the Bundschuh nappe (BK2 and BK11).

	Garnet			*Biotite*	*Muscovite*	*Phengite*	*Paragonite*	*Chlorite*	*Plagioclase*	
	core (Gt1)	*rim1 (Gt2)*	*rim2 (Gt3)*						*center*	*edge*
SiO_2	37.20	37.70	37.50	37.00	44.40	47.80	45.00	25.20	67.50	60.00
Al_2O_3	20.90	20.80	21.20	17.90	35.00	30.30	40.00	22.20	20.00	24.80
MgO	3.18	2.71	3.29	12.20	0.63	2.32	0.10	18.20	–	–
FeO	34.10	30.80	31.30	17.40	0.94	1.87	0.29	20.00	< 0.04	< 0.04
CaO	4.90	8.10	6.20	< 0.01	0.00	< 0.01	0.53	0.06	0.63	6.40
MnO	0.98	0.90	0.95	< 0.04	0.00	< 0.01	< 0.03	< 0.04	–	–
Na_2O	–	–	–	0.24	1.22	0.86	6.90	< 0.02	11.10	7.70
K_2O	–	–	–	8.30	9.30	9.40	0.57	< 0.01	0.06	0.05
TiO_2	< 0.0	0.13	< 0.05	1.45	0.67	0.55	< 0.03	< 0.05	–	–
Cr_2O_3	–	–	–	< 0.01	< 0.01	< 0.05	< 0.02	< 0.06	–	–
BaO	–	–	–	0.10	0.58	0.26	< 0.01	0.03	–	–
Cl	–	–	–	0.00	0.00	< 0.02	0.00	< 0.01	–	–
Total	101.28	101.18	100.47	94.65	92.77	93.38	93.36	85.65	99.32	98.92

Tab. 3 Representative mineral analyses from the Murau nappe (samples BK8 and BK13).

	Garnet		*Biotite*	*Muscovite*	*Chlorite*	*Plagioclase*	*Epidote*	*Ilmenite*	*Carbonates*	
	center	*edge*							*calcite*	*dolomite*
SiO_2	36.60	37.10	35.40	47.20	24.60	68.30	34.88	< 0.01	–	–
Al_2O_3	20.30	20.70	18.20	31.80	21.60	19.50	23.44	< 0.02	–	–
MgO	0.96	1.39	6.70	1.55	13.50	–	0.14	< 0.02	1.00	11.70
FeO	28.30	32.20	24.40	2.34	27.20	0.06	9.57	47.00	2.56	13.10
CaO	8.10	7.70	0.12	< 0.02	0.11	0.11	16.79	0.07	49.40	28.20
MnO	5.10	1.40	0.11	0.00	0.12	–	0.48	1.33	0.32	0.47
Na_2O	–	–	0.09	0.99	< 0.01	11.50	–	–	–	–
K_2O	–	–	8.10	9.50	< 0.01	0.03	–	–	–	–
TiO_2	0.14	0.09	1.64	0.39	< 0.05	–	0.11	52.90	–	–
Cr_2O_3	–	–	< 0.02	< 0.01	< 0.02	–	–	–	–	–
BaO	–	–	0.11	0.23	< 0.01	–	–	–	–	–
Cl	–	–	0.00	0.00	< 0.01	–	–	–	–	–
Y_2O_3	–	–	–	–	–	–	5.29	–	–	–
Total	99.58	100.63	94.77	93.94	87.04	99.46	90.70	101.31	53.26	53.39

formed biotite, muscovite and chlorite (0.4–4 mm) and quartz layers or lenses. Chlorite often forms larger (1–5 mm), randomly orientated aggregates which may be pseudomorphs or alteration products of micas. Apart from sample BK12, chlorite occurs as a rock-forming mineral (10–15 modal %). Micas overgrowing the foliation are present in a small quantity. Very fine-grained white mica aggregates (0.5–5 mm) form pseudomorphs after staurolite. They are present in most samples of the Bundschuh nappe. Several samples have been studied with the microprobe.

Sample BK2: Garnets are strongly zoned (Fig. 8 c–e). Three generations can be observed: a FeO-rich core (Gt 1) which shows more or less normal zonation in the element distribution: FeO and MgO increase (FeO: 32.2–34.2 wt%, MgO: 20.7–21.1 wt%), CaO contents decrease (CaO: 6.6–4.0 wt%) from the inner to the outer part of the core. MnO depicts an inverse zonation (MnO: 0.67–1.05 wt%). The garnet rims can be divided into an inner (Gt 2), Ca-rich (CaO: ca. 8 wt%) and an external (Gt 3), relatively Ca-poor (CaO: ca. 6 wt%) zone. There is a sudden transition in the inner rim around the almandine-rich core: The FeO content is significantly lower (FeO: 34.2–30.4 wt%), the CaO content is much higher (CaO: 4.0–8.1 wt%!) than in the core region. This inner rim-zone is enriched in inclusions, such as ilmenite, apatite and quartz. This section also shows a more or less normal zonation in the element distribution from core to rim (FeO: 30.4–31.0 wt%, MgO: 2.76–3.23 wt%, CaO at first increases, then decreases 8.1–8.9-7.8 wt%; MnO: 1.06–0.76 wt%). The Ti content is higher in the inner rim than in garnet generations 1 and 3.

Tab. 4 Representative chemical input data for thermobarometric calculations.

	BK1			BK2				BK8		BK10			
	Gr	Bi	Mu	Gr	Bi	Mu	Plag	Gr	Bi	Gr	Bi	Mu	Plag
SiO_2	36.76	35.77	46.79	37.43	36.96	45.16	62.39	36.98	35.52	37.14	36.10	46.94	62.93
Al_2O_3	20.66	19.62	32.70	21.05	18.28	34.33	23.24	20.66	18.29	20.88	17.99	31.25	22.96
MgO	3.40	10.43	1.52	3.05	11.90	0.99	–	1.23	7.06	2.36	11.45	2.13	–
FeO	36.83	18.91	1.28	31.93	17.21	1.19	0.09	31.77	23.93	30.37	18.88	1.89	0.21
CaO	1.99	0.02	0.01	6.52	0.02	0.01	4.62	8.41	0.09	8.25	0.02	0.00	4.03
MnO	0.50	0.03	0.00	0.86	0.06	0.00	–	1.78	0.12	1.09	0.07	0.00	–
Na_2O	–	0.34	1.42	–	0.25	1.44	8.90	–	0.08	–	0.17	1.04	9.37
K_2O	–	8.46	9.23	–	8.53	9.14	0.05	–	8.16	–	8.35	9.29	0.06
TiO_2	0.06	0.78	0.51	0.05	1.50	0.62	–	0.15	1.68	0.07	1.33	0.53	–
Cr_2O_3	–	0.03	0.02	–	0.04	0.02	–	–	0.03	–	0.02	0.01	–
BaO	–	0.04	0.15	–	0.13	0.57	–	–	0.07	–	0.12	0.31	–
Cl	–	0.00	0.00	–	0.00	0.00	–	–	0.00	–	0.05	0.02	–

	BK11				BK12			
	Gr	Bi	Mu	Plag	Gr	Bi	Mu	Plag
SiO_2	37.29	36.25	45.05	62.37	37.33	36.49	46.16	62.46
Al_2O_3	20.90	18.18	34.81	23.18	21.12	18.90	34.62	23.31
MgO	2.46	11.58	0.82	–	3.45	12.22	0.98	–
FeO	30.80	17.54	1.14	0.24	31.52	16.45	0.88	0.11
CaO	7.67	0.03	0.01	4.40	6.22	0.04	0.02	4.46
MnO	1.23	0.07	0.00	–	0.86	0.05	0.00	–
Na_2O	–	0.18	1.35	9.07	–	0.32	1.59	9.17
K_2O	–	8.72	9.103	0.23	–	8.42	8.79	0.07
TiO_2	0.10	1.36	0.55	–	0.06	0.95	0.39	–
Cr_2O_3	–	0.00	0.02	–	–	0.00	0.01	–
BaO	–	0.09	0.50	–	–	0.05	0.23	–
Cl	–	0.05	0.00	–	–	0.01	0.00	–

Tab. 5 Overview on P-T estimates of samples collected from Radenthein and Bundschuh nappes. The P-T estimates using geothermometers and geobarometers of KLEEMANN and REINHARDT (1994), HOISCH (1990) and HODGES and CROWLEY are listed for representative mineral compositions given in table 4.

Sample	**BK1**	**BK2**	**BK10**	**BK11**	**BK12**
Tweeq	600 °C, 11 kbar	600 °C, 9.8 kbar	600 °C, 10.3 kbar	580 °C, 9.7 kbar	630 °C, 10.3 kbar
Thermocalc	627 ± 117 °C 11.2 ± 2.6 kbar	632 ± 27 °C 10.2 ± 1.1 kbar	675 ± 43 °C 12.1 ± 1.6 kbar	631 ± 28 °C 12.7 ± 1.0	642 ± 27 °C 10.6 ± 1.1 kbar
garnet-biotite KLEEMANN and REINHARDT, 1994	604 °C	597 °C	593 °C	578 °C	607 °C
HOISCH, 1990		10.6–10.7 kbar	11.1 kbar	10.3 kbar	11.5 kbar
HODGES and CROWLEY, 1985		10.3 kbar	10.5 kbar	9.8 kbar	10.7 kbar

In the external rim, a different variation can be observed; it is, however, not as significant as that at the core-rim boundary: The CaO content is lower (CaO: 7.8–6.1 wt%), the FeO content is higher (FeO: 31.0–32.5 wt%) than in the inner rim. In the case of MnO and MgO, no considerable change was observed. The relative intensity distribution of the Ca–K_α line is shown in figure 8e.

Plagioclase often shows inverse zonation. The core is almost pure albite (X_{Ab}: ca. 0.98) and the composition is changing continuously to oligoclase (X_{An}: 0.22) in the outer zone. However this zonation is not very homogeneous, but a rather general trend as smaller, chemically different parts often occur within individual grains. Fine-grained white mica constituting the pseu-

domorphs is paragonite. Paragonite lamellae within muscovite (as in sample BK1) were not observed.

For the garnet-biotite-muscovite-plagioclase assemblage we have calculated with Tweeq conditions of ca. 600 °C and 9.8 kbar, Thermocalc gives 632 ± 27 °C and 10.2 ± 1.1 kbar.

Sample BK10: The small, idiomorphic garnets also show a well-developed, very sharp core-rim relation with the same trend as that of sample BK2 (Ca-rich rim around an almandine-rich core). Few important differences, however, are also noticeable: (1) The element distribution in the FeO-rich core is very flat for every element (Fe, Mg, Ca, Mn). This can be explained by high thermal peak conditions of metamorphism (at least 600–650 °C) that completely homogenized a possible original zonation. (2) In the rim, the element distribution shows normal zonation, but towards the edge of the grains Mn (and partly Fe as well) show opposite trends. (3) The outermost garnet generation (garnet 3) is missing. (4) The CaO content is much lower (ca. 2 wt%), the MnO content is higher (ca. 1.8 wt%) in the core than in sample BK2.

The plagioclase composition corresponds to oligoclase (X_{An}: 0.19). A zonation as in sample BK2 was not observed. Phengite represents the only white mica phase in this sample according to microprobe investigations.

Using the garnet-biotite-phengite-plagioclase assemblage calculation with Tweeq gives ca. 600 °C and 10.3 kbar, Thermocalc 675 ± 43 °C and 12.1 ± 1.6 kbar.

Sample BK11: Only a few large garnet grains show well-developed zonation, but not as symmetrical as that of BK2 and especially of BK10. The general trends are the same as within samples BK2 and BK10: FeO-rich cores (FeO: ca. 34 wt%; CaO: ca. 3 wt%), CaO-rich rims (CaO: about 7–8 wt%!; FeO: 29–30 wt%), which contain many inclusions. The almandine-rich cores contain some spots (especially near fractures) with the grossular-rich "rim composition" that makes the core rather inhomogeneous. A chemical zonation can be seen within the rim except for the MgO distribution, which is constant. The small grains are Ca-rich (CaO: ~7–8 wt%), without any noticeable zonation.

The plagioclase composition corresponds to oligoclase (X_{An}: 0.21). White micas show a wide variation in chemical composition: muscovite, phengite (and transitional compositions between muscovite and phengite) and paragonite have been identified. Phengite occurs in two textural types: (1) parallel to the foliation, and (2) crossing the foliation and muscovite as well. Paragonite is very characteristic in the abundant pseudomorphs.

Employing the garnet-biotite-muscovite-plagioclase assemblage calculation with Tweeq yields ca. 580 °C and 9.7 kbar, Thermocalc gives 631 ± 28 °C and 12.7 ± 1.0 kbar.

Sample BK12: A clear zonation in garnets is missing in this sample. A weak, rather inhomogeneous zonation similar to that in sample BK11 can be seen. A FeO-rich core region and a CaO-rich rim can be clearly established. Plagioclase and white micas (muscovite, phengite, paragonite) compositions are very similar to sample BK11.

Using the garnet-biotite-muscovite-plagioclase assemblage Tweeq yields ca. 630 °C and 10.3 kbar, Thermocalc gives 642 ± 27 °C and 10.6 ± 1.1 kbar (Fig. 9b).

4.3.3. Murau Nappe

Two garnet phyllites (Samples BK7, BK8) and a quartz-sericite-chlorite marble (sample BK13) were studied.

Samples BK7 and BK8: The garnet phyllite is a strongly foliated, fine-grained, porphyro-lepidoblastic quartz-rich phyllite. Garnet forms large (3–6 mm), cracked, pre-tectonic porphyroclasts wrapped around by the foliation. S_i is characterized by small (0.01–0.1 mm) quartz inclusions forming straight or sigmoidal trails within the garnets. The foliation is formed by the alternation of elongate (0.2–3 mm), deformed phyllosilicates (muscovite, biotite, chlorite) and "ribbon quartz" layers. Chlorite often forms asymmetric sheaths in pressure shadows of garnets. Feldspar occurs as (1) tabular porphyroclast with a diameter of 0.2–0.5 mm and (2) small (0.01–0.1 mm), oval, recrystallized grains accompanying the "ribbon quartz" layers. Small (0.1–0.5 mm), xenomorphic epidote and clinozoisite crystals are rare (< 1%), and often zoned. The core consists of Fe-rich epidote, the rim of clinozoisite. In sample BK8, calcite is also present in a small quantity, with occasionally deformation twins. Ilmenite is an accessory both as inclusions in garnets and in the rock matrix. Further accessories are apatite, zircon, tourmaline, and pyrite.

Garnet shows no core-rim structure and are relatively grossular- and spessartine-rich (X_{Alm}: 0.687, X_{Py}: 0.474, X_{Gr}: 0.233, X_{Sp}: 0.032, rim analysis). The element distribution (see also Fig. 8f) shows normal zonation (FeO: 28.2–32.6 wt%; MgO: 0.92–1.39 wt%; MnO: 5.3–1.4 wt%), except for CaO which is more or less constant at 8.5 wt%. The plagioclase is almost pure albite (X_{Ab}: 0.991, X_{An}: 0.006, X_{Or}: 0.003). White mica is muscovite;

paragonite and phengite do not appear in the rock.

In sample BK 8, garnet and biotite yield equilibrium conditions of 550–600 °C for pressures between 2 and 10 kbar (Fig. 9a).

Sample BK13: This is a foliated, fine-grained, lepido-granoblastic quartz-sericite-chlorite marble. The rock is composed mainly of calcite and dolomite with two morphological types: (1) elongate (0.2–0.8 mm), strongly twinned grains, that are mostly calcite; (2) larger (0.5–2 mm), (hyp-)idiomorphic crystals forming elongate lenses parallel to the foliation, which are generally dolomite. The foliation is constituted by alternating layers rich in carbonate and rich in orientated phyllosilicates (muscovite, chlorite). Quartz appears as separate, detrital grains with sizes of 0.1–0.4 mm or forms thin lenses or layers as "ribbon quartz". Accessories are limonite, hematite, pyrite, and ilmenite.

Mineral analyses of samples BK8 and BK13 are given in table 3. A chemical zonation was not observed in calcite, although lighter and darker parts could be distinguished in back-scattered electron images. Dolomite often has a FeO-rich (sideritic) core. Calcite-dolomite thermometry was applied (ANOVITZ and ESSENE, 1987; DACHS, 1990) and gave an equilibrium temperature of 460–500 °C for this rock.

4.3.4. Stolzalpe nappe

Sample BK14: This rock is a poorly foliated, porphyro- to lepidoblastic albite-chlorite-quartz phyllite. Large quantities (ca. 30–40%) of feldspar are present as porphyroclasts (0.1–0.8 mm) in a very fine-grained ground-mass. They are often wrapped around by the foliation with quartz fringes in their strain shadows. The matrix (0.01–0.1 mm) is composed of quartz, sericite and chlorite. Rarely larger (0.2–0.5 mm), strongly deformed quartz and mica grains can be observed. Epidote and clinozoisite occur as small (0.1–0.3 mm), xenomorphic crystals, sometimes with the same zoned structure as in BK7 and 8. Titanite forms a very abundant constituent with two textural types: (1) fine-grained aggregates (0.01–0.2 mm), and (2) larger (0.2–0.4 mm) grains with brownish pleochroism. Further accessories are apatite, zircon, tourmaline, and opaque minerals. This sample was not investigated with the microprobe.

4.3.5. Biotite compositional variations

Two chemically different biotites were identified in samples of the Middle and Upper Austroalpine units: Biotite in contact with garnet always contains more FeO and less MgO and TiO_2 than that in the matrix (parallel to the foliation), not in contact with garnet. This can be explained by incomplete metamorphic reactions with only local, "mosaic"-equilibrium conditions. The occurrence of chemically strongly different white micas among the different morphological types (described above) may also support this interpretation.

5. Discussion

Geochronological data constraining the age of the metamorphic event(s) of the investigated tectonic units are compiled in table 6 (FRIMMEL, 1986a, SCHIMANA, 1986, HAWKESWORTH, 1976). The minimum age of metamorphism in the Radenthein nappe is about 88–84 Ma according to Rb/Sr small scale whole rock and mineral isochrons. K/Ar data record an Alpine age in the Radenthein and Bundschuh (Priedröf) nappes mostly in the range of 70–110 Ma. The muscovite K/Ar age from Stangalm Mesozoic cover rocks is about 70 Ma (SCHIMANA, 1986). Bundschuh gneiss samples from sites W of Turrach (Fig. 1b) yielded ages of 363 to 403 Ma (Rb/Sr whole rock isochrons), which were interpreted as mixed Caledonian-Variscan protolith ages (FRIMMEL, 1986 a, b). Rb/Sr muscovite ages also indicate an early Variscan event (350–354 Ma) within these rocks. In orthogneisses deformed intensively during Cretaceous metamorphism, Rb/Sr mineral ages (muscovite, feldspar) are variably resetted to 119 to 91 Ma (FRIMMEL, 1986 a, b). According to these data, the Radenthein and Bundschuh tectonic units were strongly affected by Cretaceous metamorphism, while pre-Alpine metamorphism is restricted to the Bundschuh basement.

The results of the thermobarometric calculations with two different programs and thermodynamic datasets (Tweeq and Thermocalc) are roughly in agreement. Based on these data, the Alpine metamorphic conditions are estimated in the Middle Austroalpine crystalline basement (Radenthein and Bundschuh nappes) to be around 600 °C and 10–11 kbar. These values indicate upper epidote-amphibolite facies within the stability field of kyanite, although this mineral was not observed in the investigated rocks (due to the Al-poor bulk composition). However, kyanite and staurolite are found in the surrounding area in the

Tab. 6 Geochronological data from the Radenthein, Bundschuh and the Gurktal nappe complex (Sources: 1 – SCHIMANA, 1986; 2 – FRIMMEL, 1986a; 3 – HAWKESWORTH, 1976).

Tectonic unit	Lithology	Method	Mineral	Age (Ma)	Source
Bundschuh nappe	garnet-micaschist	K/Ar	muscovite	97 ± 4	1
Bundschuh nappe	garnet-micaschist	K/Ar	muscovite	140 ± 6	1
Bundschuh nappe	garnet-two-micaschist	K/Ar	muscovite	110 ± 5	1
			biotite	69 ± 4	
Bundschuh nappe	garnet-two-mica-gneiss	K/Ar	muscovite	93 ± 4	1
			biotite	101 ± 4	
Bundschuh nappe	garnet-two-mica-gneiss	K/Ar	muscovite	176 ± 7	1
Bundschuh nappe	garnet-two-mica-gneiss	K/Ar	muscovite	90 ± 4	1
Bundschuh nappe	garnet-two-mica-gneiss	K/Ar	muscovite	114 ± 5	1
			biotite	82 ± 4	
Bundschuh nappe	garnet-two-mica-gneiss	K/Ar	muscovite	135 ± 6	1
			biotite	109 ± 8	
Bundschuh nappe	orthogneiss	K/Ar	muscovite	90 ± 4	1
			muscovite	70 ± 3	
Bundschuh nappe	orthogneiss	K/Ar	muscovite	64 ± 3	1
Bundschuh nappe	orthogneiss	K/Ar	muscovite	66 ± 3	1
Bundschuh nappe	orthogneiss	Rb/Sr	whole rock	381 ± 30	2
Bundschuh nappe	orthogneiss	Rb/Sr	whole rock	394 ± 23	2
Bundschuh nappe	orthogneiss	Rb/Sr	whole rock	373 ± 30	3*
Bundschuh nappe	orthogneiss	Rb/Sr	whole rock	363 ± 27	2
Bundschuh nappe	orthogneiss	Rb/Sr	muscovite	350 ± 7	2
Bundschuh nappe	orthogneiss	Rb/Sr	muscovite	352 ± 4	2
Bundschuh nappe	orthogneiss	Rb/Sr	muscovite	354 ± 7	2
Bundschuh nappe	deformed orthogneiss	Rb/Sr	muscovite	97 ± 1	3*
Bundschuh nappe	deformed orthogneiss	Rb/Sr	muscovite	162 ± 3	2
Bundschuh nappe	deformed orthogneiss	Rb/Sr	muscovite	119 ± 2	2
Bundschuh nappe	deformed orthogneiss	Rb/Sr	muscovite-feldspar isochron	139 ± 2	2
Bundschuh nappe	deformed orthogneiss	Rb/Sr	muscovite-feldspar isochron	91 ± 1	2
Bundschuh nappe	deformed orthogneiss	Rb/Sr	muscovite-feldspar isochron	96 ± 4	2
Bundschuh nappe	amphibolite	K/Ar	hornblende	117 ± 8	1
Radenthein nappe	hornblende-garbenschist	K/Ar	muscovite	79 ± 4	1
			biotite	66 ± 3	
			hornblende	107 ± 7	
Radenthein nappe	garnet-two-micaschist	K/Ar	muscovite	78 ± 3	1
			biotite	82 ± 3	
			garnet	125 ± 20	
Radenthein nappe	garnet-micaschist	Rb/Sr	garnet-whole rock isochron	88.5 ± 3.5	1
				84 ± 1	
Stangalm Mesozoic	quartzite	K/Ar	muscovite	69 ± 3	1
Stolzalpe nappe	orthogneiss pebble	K/Ar	muscovite	295 ± 12	1
Stolzalpe nappe	orthogneiss pebble	Rb/Sr	whole rock	403 ± 20	2
Stolzalpe nappe	orthogneiss pebble	Rb/Sr	muscovite	370 ± 8	2
Stolzalpe nappe	orthogneiss pebble	Rb/Sr	muscovite	364 ± 7	2

(* Data of HAWKESWORTH corrected according to IUGS-recommended decay constants)

Radenthein nappe (kyanite-garnet micaschist with the local name "Radentheinit"; e.g., SCHIMANA, 1986). The estimated pressure suggests that these rocks were at a depth of ca. 35 km during the Cretaceous metamorphic event. This depth nearly corresponds to the base of continental crust of normal thickness.

Among the Middle Austroalpine units two types of metamorphic evolution can be identified (see also SCHIMANA, 1986): The Radenthein nappe was affected by a single, Alpine, metamorphism only, while in the Bundschuh nappe two regional (Alpine and a pre-Alpine, probably Variscan) metamorphic events are recorded. Moreover, chemical zonation (with an inner and outer garnet-rim) suggests two stages of Alpine metamorphism. The very CaO-rich inner zone of the Alpine rim in the garnets may indicate earlier,

higher pressure metamorphism when compared to the outer, Ca-poorer, zone. The albite-rich core of the zoned plagioclases may be correlated with the above mentioned inner zone; because of the absence of minerals in equilibrium, P-T conditions could not be calculated, however.

The pre-Alpine, likely Variscan, metamorphic imprint was within amphibolite facies conditions because of the presence of pseudomorphs after staurolite and of Fe-rich cores of the garnets. The element distribution in the almandine-rich cores indicates a progressive metamorphism at least in the case of sample BK2. The homogeneous element distibution in garnet-cores of sample BK10 may indicate a complete rehomogenization during the pre-Alpine metamorphic event. This would mean that garnets grew before the thermal peak of the pre-Alpine metamorphism which had

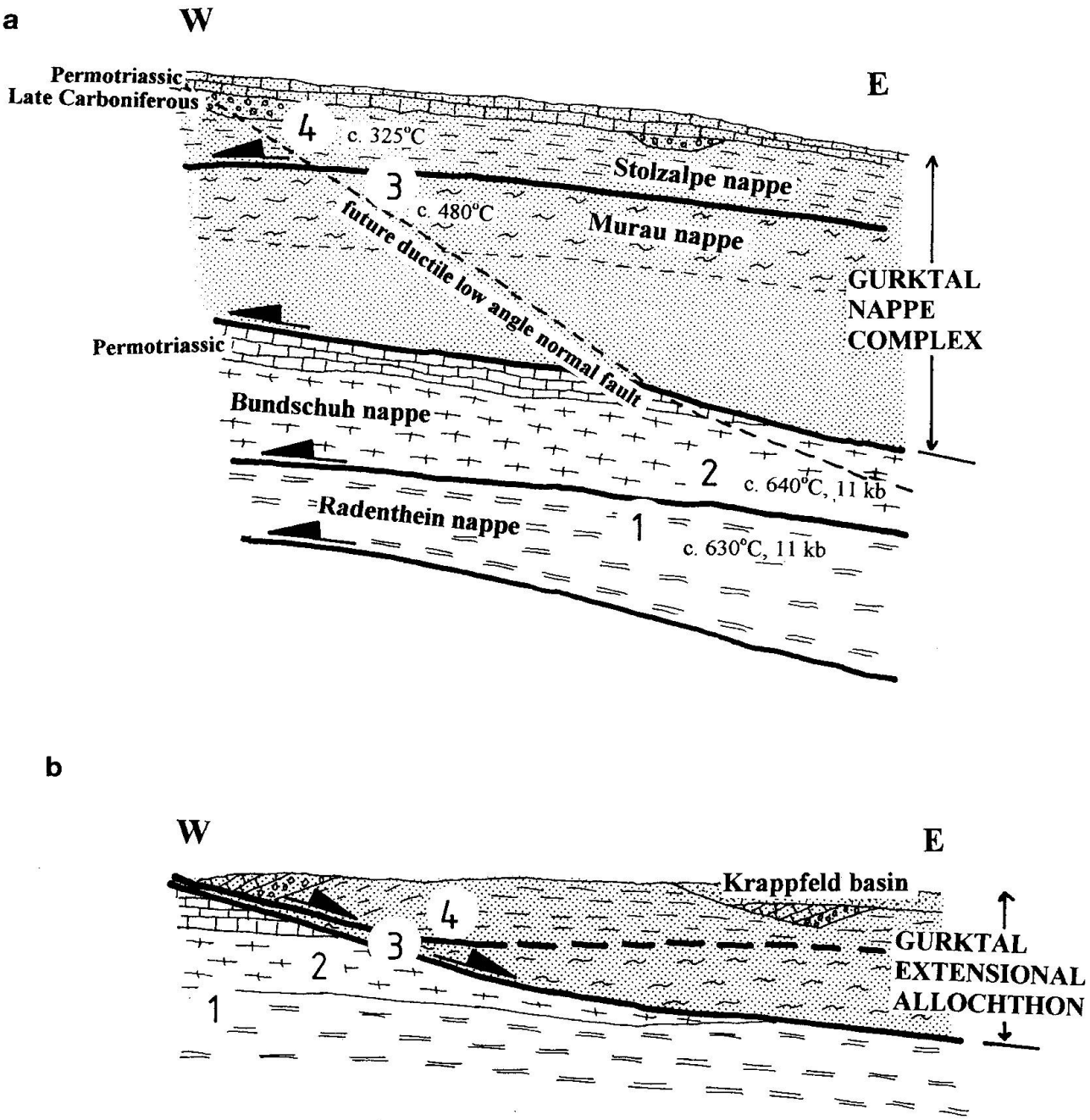

Fig. 10 Models of the tectonic evolution along the western margin of the Gurktal nappe complex. (a) Nappe stacking at the stage of maximum peak metamorphic conditions in the Bundschuh and Radenthein nappes. (b) Stage after extension by east-directed ductile low-angle normal faulting. 1–4 represent suggested locations at Cretaceous peak metamorphic conditions (a) and post-extensional locations (b) within all four investigated structural units.

to reach temperatures of at least 650 °C. The pseudomorphs containing paragonite are probably after staurolite, which is also wide-spread and well-preserved in surrounding and northwestern areas of the Bundschuh nappe (e.g., SCHIMANA, 1986). This suggests at least amphibolite facies conditions for the pre-Alpine metamorphism.

Common mineral assemblages (quartz, muscovite, chlorite, albite, ± garnet, biotite, epidote, clinozoisite, calcite, dolomite) in the Gurktaler phyllite (Murau nappe, samples BK3, 4, 6, 7, 8 and 13) and in the meta-arkose (Stolzalpe nappe, BK14) suggest greenschist facies within the Upper Austroalpine units. VON GOSEN et al. (1987) found, based on illite crystallinity studies, very low grade to low grade metamorphic conditions within the Stolzalpe nappe exposed immediately to the north of the study area. Conodont color alteration and conodont surface recrystallization studies indicate similar conditions (NEUBAUER and FRIEDL, 1997). This agrees with the presence of anthracite in the Late Carboniferous cover successions (RANTITSCH and RUSSEGGER, in prep.). A reasonable estimate for temperature conditions within the Stolzalpe nappe is, therefore, ca. 250 ± 50 °C (FREY, 1987; KISCH, 1987).

Metamorphic conditions within the Murau nappe were calculated with the calcite-dolomite thermometer (ANOVITZ and ESSENE, 1987; DACHS, 1990) which gives ca. 460–500 °C (BK13) and with garnet-biotite equilibria (BK8) yielding ca. 550–600 °C. Calcite-dolomite microfabrics are obviously associated with extensional deformation, indicating re-equilibration of calcite-dolomite mineral assemblages. The age of the metamorphism in the Murau nappe is rather uncertain, no geochronological data are available in the investigated area yet. We consider a pre-Alpine age of peak conditions of metamorphism recorded by garnet-biotite equilibria because the employed biotites are from within garnet porphyroclast (first stage of textural evolution) which are overprinted by a second-stage tectonothermal event within greenschist facies conditions. The second stage including the calcite-dolomite equilibria is considered to represent the Alpine metamorphic overprint. Similar polyphase fabrics were also reported from other regions of the Murau nappe (VON GOSEN, 1989, and references cited therein).

A break in metamorphic isograde obviously coincides with the lower low-angle normal fault boundary of the Gurktal nappe complex. It appears, furthermore, that the entire Murau nappe along the western margins of the Gurktal nappe complex is thinned out extremely (to a minimum of several tens of metres) along the east-directed ductile low angle normal fault. Further local evidence for east-directed motion has already been provided by NEUBAUER (1987), RATSCHBACHER and NEUBAUER (1989), STOCK (1989; 1992), and RATSCHBACHER et al. (1990), in each case recorded from basal sectors of the Gurktal nappe complex. Therefore, the entire Gurktal nappe complex represents an extensional allochthon. Middle Austroalpine footwall units are entirely annealed and recrystallized within a distance of several hundreds of metres in the footwall of the basal tectonic contact of the Gurktal nappe complex.

In summary, the data presented above suggest the following Cretaceous tectonic history of the Austroalpine units along the western margins of the Gurktal nappe complex:

Middle Austroalpine continental units were buried during Cretaceous contraction to depths close to the base of the continental crust (35 km). In contrast, the Murau and Stolzalpe nappes remained at middle to upper crustal levels (Fig. 10a). The direction of nappe stacking is not constrained by our data except some weak indications of westward rotation recorded in garnets of the Radenthein nappe. Later, a crustal-scale, east-directed, ductile low-angle normal fault developed at the upper margin of the Bundschuh nappe probably reactivating older thrust surfaces. A late stage brittle normal fault has already been described by CLAR (1965) along this contact. Mineral cooling ages of 84–80 Ma from Bundschuh and Radenthein nappes (HAWKESWORTH, 1976; SCHIMANA, 1986; FRIMMEL, 1986 a, b) are contemporaneous with sediment deposition within the Late Cretaceous Krappfeld Gosau basin (VAN HINTE, 1963; THIEDIG, 1975) on top of the Stolzalpe nappe along the eastern margin of the present exposure of the Gurktal nappe complex (Fig. 1b).

The tectonic scenario derived from these investigations in the Gurktal nappe complex is similar to that described from other regions of the Austroalpine nappe complex exposed east and west of the Tauern window, where east-directed Late Cretaceous syn-Gosau normal faulting is recorded (e.g., NEUBAUER and GENSER, 1990; RATSCHBACHER et al., 1991; FROITZHEIM et al., 1994, 1997; NEUBAUER et al., 1995; HANDY, 1996).

Acknowledgements

We acknowledge discussions with Edgar Dachs who helped to avoid pitfalls with using Tweeq and Thermocalc programs. We appreciate thorough reviews by Christian de Capitani and Niko Froitzheim, and suggestions by Arnold Stahel. The work has been supported by a grant (FWF P9918-GEO "Collisional Orogen") of the Austrian Research Foundation.

References

ANGELIER, J. and MECHLER, P. (1977): Sur une méthode graphique de recherche des contraintes principales également utilisable en tectonique et en séismologie: la méthode des dièdres droits. Bull. Soc. Géol. France, VII, 19, 1309–1318.

ANOVITZ, L.M. and ESSENE, E.J. (1987): Phase equilibria in the system $CaCO_3$–$MgCO_3$–$FeCO_3$. J. Petrol., 28, 389–414.

ANTONITSCH, W. and NEUBAUER, F. (1992): Altpaläozoischer alkalischer Riftvulkanismus und kretazische Imbrikation in der westlichen Gurktaler Decke, Ostalpen. Frankf. Geowiss. Abh., A11, 15–18.

BERMAN, R.G. (1990): Mixing properties of Ca–Mg–Fe–Mn garnets. Am. Miner. 75, 328–344.

BERMAN, R.G. (1991): Thermobarometry using multi-equilibrium calculations: A new technique with petrological applications. Can. Mineral., 29, 833–855.

CHATTERJEE, N.D. and FROESE, E. (1975): A thermodynamic study of the pseudo-binary join muscovite-paragonite in the system $KAlSi_3O_8$–$NaAlSi_3O_8$–Al_2O_3–SiO_2–H_2O: new phase equilibria data, some calculated phase relations, and their petrological applications. Contrib. Mineral. Petrol., 88, 1–13.

CHOUKROUNE, P., GAPAIS, D. and MERLE, O. (1987): Shear criteria and structural symmetry. J. Struct. Geol., 9, 525–530.

CLAR, E. (1965): Zum Bewegungsbild des Gebirgsbaues der Ostalpen. Z. Deutsch. Geol. Ges. 116, 267–291.

DACHS, E. (1990): Geothermobarometry in metasediments of the southern Grossvenediger area (Tauern Window, Austria). J. Met. Geol., 8, 217–230.

DALLMEYER, R.D., NEUBAUER, F., HANDLER, R., FRITZ, H., MÜLLER, W., PANA, D. and PUTIS, M. (1996): Tectonothermal evolution of the internal Alps and Carpathians: Evidence from $^{40}Ar/^{39}Ar$ mineral and whole-rock data. Eclogae geol. Helv. 89, 203–227.

DALLMEYER, R.D., HANDLER, R., NEUBAUER, F. and FRITZ, H. (1998): Sequence of thrusting within a thick-skinned tectonic wedge: evidence from $^{40}Ar/^{39}Ar$ and Rb–Sr ages from the Austroalpine nappe complex of the Eastern Alps. J. Geol., 106, 71–86.

EHLERS, K., STÜWE, K., POWELL, R., SANDIFORD, M. and FRANK, W. (1994): Thermometrically inferred cooling rates from the Plattengneis, Koralm region, Eastern Alps. Earth Planet. Sci. Lett., 125, 307–321.

ENGLAND, P.C. and THOMPSON, A.B. (1984): Pressure-temperature-time paths of regional metamorphism. Part I: Heat transfer during the evolution of regions of thickened continental crust. J. Petrol., 25, 894–928.

FRANK, W. (1987): Evolution of the Austroalpine elements in the Cretaceous. In: FLÜGEL, H.W. and FAUPL, P. (eds): Geodynamics of the Eastern Alps. Deuticke, Wien, 379–406.

FRANK, W., KRALIK, M., SCHARBERT, S. and THÖNI, M. (1987): Geochronological Data from the Eastern Alps. In: FLÜGEL, H.W., and FAUPL, P. (eds): Geodynamics of the Eastern Alps. Deuticke, Wien, 272–279.

FREY, M. (1987): Very low-grade metamorphism of clastic sedimentary rocks. In: FREY, M. (ed.): Low temperature metamorphism. Chapman and Hall, New York, 9–58.

FRIMMEL, H. (1986a): Petrographie, Gefügemerkmale und geochronologische Daten von Kristallingeröllen aus dem Oberkarbon der Gurktaler Decke im Vergleich zum benachbarten Altkristallin. Mitt. Ges. Geol. Bergbaustud. Österr., 32, 39–65.

FRIMMEL, H. (1986b): Isotopengeologische Hinweise für die paläogeographische Nachbarschaft von Gurktaler Decke (Oberostalpin) und dem Altkristallin östlich der Hohen Tauern (Österreich). Schweiz. Mineral. Petrogr. Mitt., 66, 193–208.

FRIMMEL, H. (1988): Metagranitoide am Westrand der Gurktaler Decke (Oberostalpin) – Genese und paläotektonische Interpretation. Jb. Geol. Bundesanst., 131, 575–592.

FROITZHEIM, N., SCHMID, S.M. and CONTI, P. (1994): Repeated change from crustal shortening to orogen-parallel extension in the Austroalpine units of Graubünden. Eclogae geol. Helv., 87, 559–612.

FROITZHEIM, N. SCHMID, S.M. and FREY, M. (1996): Mesozoic palaeogeography and the timing of eclogite-facies metamorphism in the Alps: A working hypothesis. Eclogae geol. Helv., 89, 81–110.

FROITZHEIM, N., CONTI, P. and VAN DAALEN, M. (1997): Late Cretaceous, synorogenic, low-angle normal faulting along the Schlinig fault (Switzerland, Italy, Austria) and its significance for the tectonics of the Eastern Alps. Tectonophysics, 280, 267–293.

FUHRMAN, M.L. and LINDSLEY, D.H. (1988): Ternary feldspar modeling and thermometry. Amer. Mineral., 73, 201–215.

HANMER, S. and PASSCHIER, C.W. (1991): Shear sense indicators: a review. Geol. Surv. Can. Pap., 90, 1–71.

HANDY, M.R. (1996): The transition from passive to active margin tectonics: a case study from the zone of Samedan (Eastern Switzerland). Geol. Rdsch., 85, 832–851.

HAWKESWORTH, C.J. (1976): Rb/Sr Geochronology in the Eastern Alps. Contrib. Mineral. Petrol., 54, 225–244.

HODGES, K.V. and CROWLEY, P.D. (1985): Error estimates and empirical geobarometry for pelitic systems. Amer. Mineral., 72, 671–680.

HOISCH, T.D. (1991): Equilibria within the mineral assemblage quartz-muscovite-biotite-garnet-plagioclase and implications for the mixing properties of octohedrally coordinated cations in muscovite and biotite. Contrib. Mineral. Petrol., 108, 43–54.

HOLDHAUS, K. (1921): Über die Auffindung von Trias im Königstuhlgebiet in Kärnten. Anz. Akad. Wiss. Wien, math.-naturwiss. Kl., 58, 19–21.

KISCH, H.J. (1987): Correlation between indicators of very low-grade metamorphism. In: FREY, M. (ed.): Low temperature metamorphism. Chapman and Hall, New York, 227–300.

KLEEMANN, U. and REINHARDT, J. (1994): Garnet-biotite thermometry revisited: the effect of Al^{VI} and Ti in biotite. Eur. J. Mineral., 6, 925–941.

MCMULLIN, D.W.A., BERMAN, R.G. and GREENWOOD, H.J. (1991): Calibration of the SGAM thermobarometer for pelitic rocks using data from phase-equilibrium experiments and natural assemblages. Can. Mineral., 29, 889–908.

MESCHEDE, M. (1995): Methoden der Strukturgeologie. Enke-Verlag, Stuttgart.

MILLER, C. (1990): Petrology of the type locality eclogites from the Koralpe and Saualpe (Eastern Alps), Austria. Schweiz. Mineral. Petrogr. Mitt., 70, 287–300.

NEUBAUER, F. (1980): Zur tektonischen Stellung des Ackerlkristallins (Nordrand der Gurktaler Decke). Mitt. Österr. Geol. Ges., 73, 39–53.

NEUBAUER, F. (1987): The Gurktal Thrust System within the Austroalpine region – some structural and geometrical aspects. In: FLÜGEL, H.W. and FAUPL, P. (eds): Geodynamics of the Eastern Alps. Deuticke, Wien, 226–236.

NEUBAUER, F. (1994): Kontinentalkollision in den Ostalpen. Geowissenschaften, 12, 136–140.

NEUBAUER, F. and FRIEDL, G. (1997): Conodont preservation within the Gurktal nappe complex, Eastern Alps. Zentralbl. Geol. Paläont. Teil II, 1997, 277–289.

NEUBAUER, F. and GENSER, J. (1990): Architektur und Kinematik der östlichen Zentralalpen – eine Übersicht. Mitt. Naturwiss. Steiermark, 120, 203–219.

NEUBAUER, F. and PISTOTNIK. J. (1984): Das Altpaläozoikum und Unterkarbon des Gurktaler Deckensystems (Ostalpen) und ihre paläogeographischen Beziehungen. Geol. Rundsch., 73, 149–174.

NEUBAUER, F., DALLMEYER, R.D., DUNKL, I. and SCHIRNIK, D. (1995): Late Cretaceous exhumation of the metamorphic Gleinalm dome, Eastern Alps: kinematics, cooling history and sedimentary response in a sinistral wrench corridor. Tectonophysics, 242, 79–98.

PETIT, J.P. (1987): Criteria for the sense of movement on fault rock surfaces in brittle rocks. J. Struct. Geol., 9, 597–608.

POWELL, R. and HOLLAND, T.J.B. (1988): An internally consistent thermodynamic dataset with uncertanities and correlations. III. Application methods, worked examples and a computer program. J. metam. Geol., 6, 173–204.

RANTITSCH, G. and RUSSEGGER, B. (in prep.): Thrust-related very low grade metamorphism within the Gurktal nappe complex (Eastern Alps). Geol. Rdsch. (submitted).

RATSCHBACHER, L. and NEUBAUER, F. (1989): West-directed decollement of Austro-Alpine cover nappes in the eastern Alps: geometrical and rheological considerations. Geol. Soc. Spec. Publ., 45, 243–262.

RATSCHBACHER, L., FRISCH, W., NEUBAUER, F., SCHMID, S.M. and NEUGEBAUER, J. (1989): Extension in compressional orogenic belts: The eastern Alps. Geology, 17, 404–407.

RATSCHBACHER, L., SCHMID, S.M., FRISCH, W. and NEUBAUER, F. (1990): Reply on the Comment of S.R. Wallis to Extension in compressional orogenic belts: the eastern Alps. Geology, 18, 675–676.

SCHIMANA, R. (1986): Neue Ergebnisse zur Entwicklungsgeschichte des Kristallins um Radenthein (Kärnten, Österreich). Mitt. Ges. Geol. Bergbaustud. Österr., 33, 221–232.

SIMPSON, C. and SCHMID, S.M. (1983): An evaluation of criteria to deduce the sense of movement in sheared rocks. Geol. Soc. Amer. Bull., 94, 1281–1288.

STOCK, P. (1989): Zur antithetischen Rotation der Schieferung in Scherbandgefügen – ein kinematisches Deformationsmodell mit Beispielen aus der südlichen Gurktaler Decke (Ostalpen). Frankfurter Geowiss. Arb., A7, 1–155.

STOCK, P. (1992): A strain model for antithetic fabric rotation in shear band structures. J. Struct. Geol., 14, 1267–1275.

THIEDIG, F. (1975): Submarine Brekzien als Folge von Felsstürzen in der Turbidit-Fazies der Oberkreide des Krappfeldes in Kärnten (Österreich). Mitt. Geol.-Paläont. Inst. Univ. Hamburg, 44, 495–516.

TOLLMANN, A. (1975): Die Bedeutung des Stangalm-Mesozoikums in Kärnten für die Neugliederung des Oberostalpins in den Ostalpen. N. Jb. Geol. Paläont. Mh., 150, 19–43.

TOLLMANN, A. (1977): Geologie von Österreich. Band 1. Die Zentralalpen. XVI + 710 pp., Vienna (Deuticke).

TOLLMANN, A. (1987): The Alpidic Evolution of the Eastern Alps. In: FLÜGEL, H.W. and FAUPL, P. (eds): Geodynamics of the Eastern Alps. Deuticke, Wien, 361–378.

VAN HINTE, J.E. (1963): Zur Stratigraphie und Mikropaläontologie der Oberkreide und des Eozäns des Krappfeldes (Kärnten). Jb. Geol. Bundesanst. Sdbd., 8, 1–147.

VON GOSEN, W. (1989): Gefügeentwicklungen, Metamorphosen und Bewegungen der ostalpinen Baueinheiten zwischen Nockgebiet und Karawanken (Österreich). Geotekt. Forsch., 72, 1–247.

VON GOSEN, W., PISTOTNIK, J. and SCHRAMM, J.M. (1987): Schwache Metamorphose in Gesteinsserien des Nockgebietes und im Postvariszikum des Karawankenvorlandes (Ostalpen, Kärnten). Jb. Geol. Bundesanst., 130, 31–36.

WALLBRECHER, E. and UNZOG, W. (1993): Gefüge 5 (Version 5.0): Ein Programmpaket zur Behandlung von Richtungsdaten. Dept. of Geology, University of Graz.

Manuscript received May 26, 1997; revision accepted December 21, 1998.